HHS Public Access

Author manuscript

Nanotechnology. Author manuscript; available in PMC 2016 March 20.

Published in final edited form as:

Nanotechnology. 2015 March 20; 26(11): 115603. doi:10.1088/0957-4484/26/11/115603.

Silk-regulated hierarchical hollow magnetite/carbon nanocomposite spheroids for lithium ion battery anodes

Weiqin Sheng[a], **Guobin Zhu**[b], **David L Kaplan**[a,c], **Chuanbao Cao**[d], **Hesun Zhu**[d], and **Qiang Lu**[a]

Qiang Lu: Lvqiang78@suda.edu.cn

[a]National Engineering Laboratory for Modern Silk & Collaborative Innovation Center of Suzhou Nano Science and Technology, Soochow University, Suzhou 215123, People's Republic of China

[b]College of Physics, Optoelectronics and Energy & Collaborative Innovation Center of S uzhou Nano Science and Technology, Soochow University, Suzhou 215006, People's Republic of China

[c]Department of Biomedical Engineering, Tufts University, Medford, MA 02155, USA

[d]Research Center of Materials Science, Beijing Institute of Technology, Beijing 100081, People's Republic of China

Abstract

Hierarchical olive-like structured carbon-Fe_3O_4 nanocomposite particles composed of a hollow interior and a carbon coated surface are prepared by a facile, silk protein-assisted hydrothermal method. Silk nanofibers as templates and carbon precursors first regulate the formation of hollow Fe_2O_3 microspheres and then they are converted into carbon in a reduction process into Fe_3O_4. This process significantly simplifies the fabrication and carbon coating processes to form complex hollow structures. When tested as anode materials for lithium-ion batteries, these hollow carbon-coated particles exhibit high capacity (900 mAh g^{-1}), excellent cycle stability (180 cycles) and rate performance due to their unique hierarchical hollow structure and carbon coating.

Keywords

Fe_3O_4; olive-like hollow structures; silk nanofiber; energy storage; anode material

1. Introduction

Lithium-ion batteries (LIBs), the dominant power sources for portable electronic devices [1–4], are expanding their applications to electric vehicles and green energy grids [5–9]. The growing demand for these emerging applications boosts continuing interest in seeking more environmentally acceptable anode materials with high energy and power density and long life-times [10]. Among the available alternative anode materials, magnetite is a promising candidate due to its higher theoretical capacity (926 mAh g^{-1}) than graphite and other transition metal oxides such as SnO_2 [11], high electronic conductivity (2×10^4 S m^{-1}),

Correspondence to: Qiang Lu, Lvqiang78@suda.edu.cn.

nontoxicity, low cost, abundance, and environmental compatibility [12–16]. Despite these attractive features, the large capacity decay caused by the large volume expansion of Fe_3O_4 during charge-discharge hinders its practical applications for LIBs [17]. Different approaches have been developed to overcome these problems. One strategy is to fabricate Fe_3O_4 hollow nanostructures with high area and short diffusion paths, leading to a better rate capacity and improved cycling stability [18, 19]. Other solutions are to coat or encapsulate magnetite with carbon, which can increase electrical conductivity, and alleviate pulverization and aggregation of the magnetite materials [20–23]. Although some exciting developments have been achieved in recent studies, the fabrication of truly durable Fe_3O_4 anodes with high-rate capability and high specific capacity remains a challenge.

The construction of a hierarchical hollow nanostructure of Fe_3O_4/carbon composite might be a good approach to address the current issues and challenges. It is expected that more efficient and rapid transfer of ions and electrons, and the accommodation of volume expansion during cycling, could be achieved via this approach. However, it remains a challenge to develop a simple, green and reliable method for the formation of such hierarchical nanostructures. Most template-assisted methods for the formation of hollow structures involve complicated procedures including the preparation and removal of templates [24, 25]. Furthermore, the production of Fe_3O_4/carbon composite materials requires a complicated process. Few successful attempts have been reported to design hollow Fe_3O_4/carbon nano-composites with enhanced lithium storage properties.

Bombyx mori silk fibroin (SF), a naturally derived, high molecular weight, amphiphilic protein polymer, has unique self-assembly behavior, excellent biocompatible and mechanical property, acting as a template to prepare different nanomaterials such as calcium carbonate [26], copper oxide [27], silver [28], and iron oxides [29, 30] with controllable morphologies. However, reliable control of nanostructures of SF-regulated materials is challenging due to the polymorphic and dynamic state of the silk chains in solution. This problem was addressed by tuning the self-assembly process of SF in our recent study [31]. Water dispersible SF nanofibers with high beta-sheet content were prepared, providing a stable template for the formation of different nanomaterials including iron oxides. Herein, we report a facile and scalable solvothermal method for synthesizing hierarchical olive-like Fe_3O_4/carbon hollow microspheres via the assistance of the templating SF nanofibers. The hollow microspheres were prepared by a simple one-pot reaction with the SF nanofibers as templates, followed by calcination at 600°C in Ar where the SF nanofiber was used as a carbon precursor without additional separation or purification steps. The multiple functions of the SF nanofiber simplified previous complicated steps in hollow structural fabrication and carbon coating processes, resulting in the reliable preparation of hollow Fe_3O_4/carbon nanocomposite particles with excellent capacity, cycle stability, and rate performance.

2. Experimental

2.1. Materials

Iron (III) chloride hexahydrate ($FeCl_3{\cdot}6H_2O$), Ethanol and Na_2CO_3 were purchased from Sinopharm Chemical Reagent Co., Ltd., Shanghai, China. LiBr was purchased from Sigma-Aldrich. All the reagents were used without further purification.

2.2. Preparation of silk fibroin solutions

SF solutions were prepared according to our previously published procedures [32]. *B. mori* cocoons were boiled for 20 min in an aqueous solution of 0.02 M Na_2CO_3 and then rinsed thoroughly with deionized water to extract the sericin proteins. After drying, the extracted silk was dissolved in 9.3 M LiBr solution at 60 °C for 4 h, yielding a 20% (w/v) solution, since LiBr could dissolve the crystalline regions of silk fibroin and then make silk fibroin soluble in water. This solution was dialyzed against deionized water using dialysis tube (MWCO 3,500) for 72 h to remove the salt. Then the solution was centrifuged at 9,000 rpm for 20 min at 4 °C to remove silk aggregates formed during the process. The final concentration of silk was about 7 wt%, determined by weighing the remaining solid after drying. The prepared SF solution was stored at 4 °C for future use.

2.3. Preparation of silk fibroin nanofiber solutions

SF nanofiber solutions were prepared according to our recent work [31]. Typically, the SF solution was concentrated to about 20% (w/w) over 24 h at 60 °C to form metastable nanoparticles. Then the concentrated SF solution was diluted to 0.5% with deionized water and incubated at 60 °C until the SF nanofiber solution formed.

2.4. Synthesis of olive-like Fe_3O_4/C hollow microspheres

Olive-like hollow microspheres were synthesized by a simple solvothermal method. In a typical procedure, the SF nanofiber solution was sonicated with a SL-650D Sonifier for 10 min at 80% amplitude (output power supply is 650 W) to achieve short nanofiber templates (diameter 20nm, length 100–200nm) (Figure S1, Supporting Information). Then, 1.2g $FeCl_3{\cdot}6H_2O$ was dissolved in the 90 ml sonicated SF solution with stirring. The transparent mixture was transferred to a 100 ml Teflon-lined stainless-steel autoclave and heated at 160 °C for 20 h. After the autoclave was cooled to room temperature, the as-prepared α-Fe_2O_3/SF hollow microspheres were collected after a centrifugal process (8,000 rpm, 30 min), and washing process with deionized water and ethanol for three times each, followed by drying in a vacuum oven at 60 °C for 12 h. Different weights of $FeCl_3{\cdot}6H_2O$ were also added into the above sonicated SF solution to achieve α-Fe_2O_3/SF microspheres with various morphologies and sizes. The olive-like α-Fe_2O_3/SF hollow microspheres obtained were then calcined at 600 °C in Ar for 5 h to generate olive-like Fe_3O_4/C hollow structures.

2.5. Characterizations

X-ray diffraction (XRD) patterns of the samples were recorded on an X'Pert-Pro diffractometer (PANalytical, Holland) with Cu Kα radiation in the 2θ range from 10 to 90° at 40 kV and 40 mA. TEM and high-angle annular dark-field scanning TEM (HAADF-STEM) were performed using a Tecnai FEI 20 transmission electron microscope (Tecnai G2 F20, FEI, USA) at 200kV. In addition, field emission scanning electron microscopy (FESEM, SU8010, Hitachi, Japan) was used to determine morphology at 15kV. The sample solutions were dipped on the Cu grids for TEM observation, and similarly were cast on silicon wafers for SEM characterization.

2.6. Electrochemical measurements

Electrochemical measurements were carried out using pure lithium foil as the counter/reference electrode, polypropylene (Celgard 2400) film as the separator, Fe_3O_4/C as the working electrode, and 1M $LiPF_6$ dissolved in ethylene carbonate (EC)/diethyl carbonate (DEC) (1:1 v/v) as the electrolyte. The Fe_3O_4/C working electrode was prepared by mixing 65% of the active material (Fe_3O_4/C), 25% of the conducting carbon black (super-P-Li) and 10% of polyvinylidenedifluoride (PVDF). The cells were assembled in a glove box filled with argon. The galvanostatic charge-discharge cycles were tested by a LAND CT2001A (Wuhan, China) battery tester at 303K, respectively.

3. Results and discussion

The chemical composition and phase purity of the calcined product is determined by XRD analysis. All diffraction peaks in the XRD pattern can be unambiguously assigned to the Fe_3O_4 phase (JCPDS card no. 03-065-3107) (Figure 1a). No other impurities are observed. The typical black colour of the product further confirms the formation of Fe_3O_4. The Fe_3O_4 particles were characterized by FESEM (Figure 1b) and showed uniform olive-like particles with a length of about 1.0 μm and a diameter of about 500 nm. From the cross-section images (Figure 1c, polished by Iion, Gatan 693 Precision Cross-Section System), the hollow particles with volume ratio of about 50% were composed of densely packed subunits. The high-magnification TEM image (Figure 1d) of the shell of the particles shows a thin carbon coating with depth of about 1nm outside the Fe_3O_4 shell (Figure 1e), which will facilitate electrical conductivity and alleviate pulverization and aggregation of the magnetite spheres.

The uncalcined precursor particles obtained in the presence of SF nanofibers in the reaction mixture are characterized by XRD and FESEM (Figure S2). The morphological comparison between the precursor and final Fe_3O_4 particles shows no noticeable structural change caused by the calcination process. The XRD pattern (Figure S2a) shows typical diffraction peaks of α-Fe_2O_3 (JCPDS card no. 00-024-0072), which is further confirmed with the red colour of the powder in a mortar, the typical colour of α-Fe_2O_3 particles. We therefore conclude that the as-prepared precursor is hematite that is converted into Fe_3O_4 phase in Ar by the reduction of carbon carbonized from SF [20].

In the present solvothermal system, the SF nanofiber additive has an important influence on the morphology of the product. We therefore study the effect of different amounts of SF nanofibers in the reaction mixture on the structure of the α-Fe_2O_3 particles before calcination (Figure 2). When less silk nanofiber (the ratio of SF to $FeCl_3{\cdot}6H_2O$, 2:9 (w/w)) is present in the reaction system, the particles obtained are olive-like structures with a larger size (about 2 μm in length, 1.2 μm in diameter). Following the increase of SF (the ratio of SF to $FeCl_3{\cdot}6H_2O$, 6:5 (w/w)) in the reaction mixture, the α-Fe_2O_3 particles maintain an olive-like morphology with a decrease in size from several microns to about 100 nanometers, and are finally transformed into irregular nanoparticles with a size of about several ten nanometers. It is also observed that the hollow structure change when more silk nanofiber is present in the reaction system. If the relative amount of SF nanofiber to $FeCl_3{\cdot}6H_2O$ is increased to more than 4/7 (w/w), a dense packing of the nanoparticle subunits appear, giving the structure an almost solid interior (Figure S3). These observations suggest that the

formation of olive-like hollow spheres composed of smaller nanoparticles depend primarily on the concentration of SF in the reaction system.

We next carry out a time-dependent experiment to clarify the formation process of the unique hollow olive-like structures in the present system. Nanorods with a similar length to the silk nanofiber templates are collected after a reaction time of 1h and 2h. When the reaction duration is prolonged to 6 h, olive-like spheres have formed. Scheme 1 illustrates the formation process of the precursor olive-like hollow α-Fe_2O_3 spheres. The tyrosine residues in SF macromolecular chains can provide strong interactions with Fe (III) [33, 34], making silk-Fe complexes possible in different reaction systems. Compared to previous reported silk fibroin materials, silk fibroin nanofiber with increased negative potential provided stronger interactions with positive charged Fe (III) [35] to form silk-Fe nanofiber complexes. Then the silk-Fe nanofiber complexes are hydrolyzed into FeOOH during the hydrothermal process, and the FeOOH nanoparticles are further dehydrated to transform into olive-like α-Fe_2O_3, accompanied by the reassembly and aggregation process to reduce the system energy. The FeOOH firstly assembled into nanofiber structure and then aggregated to form olive-like structure rather than microspheres due to the influence of the SF nanofiber template (as opposed to free silk protein chains in solution) [36]. During longer reaction times, the small α-Fe_2O_3 crystallites in the core region of the spheres are dissolved according to an inside-out Ostwald ripening process [5]. The hollowing process continues with longer reaction times until well-defined olive-like hollow spheres form. The HAADF-STEM images (Figure 3) reveal the hollowing process. The spheres obtained after reaction for 6 h are still solid. When the reaction time is extended to 8 h, hollow structures initially appear around the central region of the spheres. After 20 h, well-defined olive-like hollow spheres form.

The calcination and reduction happen simultaneously at 600 °C for 5 h in Ar to form hierarchical olive-like Fe_3O_4/carbon hollow microspheres in the reaction system. Our previous studies have revealed that SF regulate crystallization, serving as a template, and also coat the outside the particles as a stabilizer [26, 35]. The SF coating also form outside the α-Fe_2O_3 particles (Figure 3i, insert), and help with the formation of the hierarchical hollow magnetite spheres with carbon coatings after calcination and reduction at 600 °C in Ar. We next study the electrochemical properties of the carbon-coated hollow magnetite spheres. Figure 4a presents the results of the electrochemical tests conducted by galvanostatic charge-discharge voltage cycling between 50 mV and 3.0 V (*versus* Li^+/Li) at a current density of 200 mA g^{-1}. A distinct voltage plateau is identified at about 0.75 V, agreeing well with that found in prior studies [20, 23]. This conversion -reaction provide the dominant contribution to the lithium-storage capacity of the material. The first discharge and charge capacities are 1369 mAh g^{-1} and 1028 mAh g^{-1}, respectively, leading to a relatively low irreversible capacity loss of 25%. Such initial irreversible capacity loss is usually due to the formation of a solid-electrotyte interface (SEI) and some side reactions [20, 23]. The Coulombic efficiency increases rapidly to 97% in the second cycle and stabilize to 99% over 180 cycles, indicating the irreversible surface reactions are limited by the hollow structure and carbon coating of the material. The cycling performance and Coulombic efficiency of the material are further evaluated by prolonging cycling over 180 cycles at a constant

current density of 200 mA g^{-1} between 50 mV and 3.0 V (Figure 4b). As expected, the as-prepared hierarchical Fe_3O_4/carbon hollow spheres exhibit excellent cyclic capacity retention with a stable reversible capacity of about 900 mAh g^{-1} even at the end of 180 charge-discharge cycles. The rate performance of the sample is examined by charging/discharging the cells at different current densities from 0.1C, 0.2C, 0.5C, 1C, 2C, 5C, 10C, 20C, and back to 0.1C and 1C (1 C = 1000 mA g^{-1}) for 3 cycles interval each (Figure 4c). The ultrahigh specific capacity of the Fe_3O_4/carbon hollow spheres steadily decrease as the current rate is increased, which is possibly due to the slow diffusion of Li^+ ions in the solid material. However, the capacity returns to 950 mAh g^{-1} from 374 mAh g^{-1} when the current rate is reassumed to 1 C, suggesting that the electrode materials could sustain the extensive cycling at high rates. It is particularly interesting to note that the specific capacity of the Fe_3O_4/carbon hollow spheres at different current densities has been enhanced when compared to olive-like Fe_3O_4/carbon solid spheres (Figure S4) and other hollow Fe_3O_4 spheres-based electrodes under similar conditions [12, 19]. We can attribute this superior performance to the carbon coating providing fast and efficient transport of Li ions.

Thus, the advantage of the present material for energy storage is apparent. The electrochemical performance, including the high specific capacity, enhanced cycling stability and rate performance, relate to the advantageous structure of these hierarchical hollow Fe_3O_4/carbon nanocomposite spheres. The hollow interior endows the spheres with high structural integrity and efficient transport of Li ions because of the effective buffer of the stress induced during charge-discharge process and the short Li ion diffusion length. The carbon coating further relieves the stress induced by volume expansion/contraction and increases the electrical conductivity. These Fe_3O_4/carbon hollow microspheres have potential as an interesting anode material.

4. Conclusions

A simple SF nanofiber-assisted solvothermal method for the synthesis of hierarchical olive-like Fe_3O_4/carbon hollow microspheres was identified. SF nanofibers served as templates to first control the morphology of α-Fe_2O_3 precursors, inducing olive-like hollow microsphere formation. These precursor hollow microspheres could be readily converted into Fe_3O_4 hollow microspheres by reduction under an Ar atmosphere without significant structural collapse. In the process, silk nanofibers as a carbon precursor are converted into carbon that coats the outside the spheres. In view of their unique structural advantages, these olive-like Fe_3O_4/carbon hollow microspheres were evaluated as an anode material for lithium-ion batteries, showing improved electrochemical performance with excellent cycling stability and a higher reversible capacity of 900 mA h g^{-1} even after 180 cycles.

Supplementary Material

Refer to Web version on PubMed Central for supplementary material.

Acknowledgements

We thank National Basic Research Program of China (973Program, 2013CB934400), NSFC (21174097, 81272106, 81271412), and the NIH (R01 DE017207). We also thank the Priority Academic Program Development of Jiangsu

Higher Education Institutions (PAPD), the Excellent Youth Foundation of Jiangsu Province (BK2012009), International S&T Cooperation Project of the Ministry of S&T of China (2010DFR30850) and the Key Natural Science Foundation of the Jiangsu Higher Education Institutions of China (11KGA430002) for support of this work.

References

1. Armand M, Tarascon JM. Nature. 2008; 451:652. [PubMed: 18256660]
2. Tarascon JM, Armand M. Nature. 2001; 414:359. [PubMed: 11713543]
3. Chen JS, Archer LA, Lou XW. J. Mater. Chem. 2011; 21:9912.
4. Wang B, Chen JS, Wu HB, Wang ZY, Lou XW. J. Am. Chem. Soc. 2011; 133:17146. [PubMed: 21977903]
5. Zhu J, Ng KYS, Deng D. ACS Appl. Mater. Interfaces. 2014; 6:2996. [PubMed: 24467218]
6. Jeong JM, Choi BG, Lee SC, Lee KG, Chang SJ, Han YK, Lee YB, Lee HU, Kwon S, Lee GH, Lee CS, Huh YS. Adv. Mater. 2013; 25:6250. [PubMed: 23966264]
7. Yoshino A. Angew. Chem. Int. Ed. 2012; 51:5798.
8. Bruce PG, Freunberger SA, Hardwick LJ, Tarascon JM. Nat.Mater. 2012; 11:19. [PubMed: 22169914]
9. Dunn B, Kamath H, Tarascon JM. Science. 2011; 334:928. [PubMed: 22096188]
10. Wang ZY, Luan DY, Madhavi S, Hu Y, Lou XW. Energy Environ. Sci. 2012; 5:5252.
11. Tian QH, Tian Y, Zhang ZX, Yang L, Hirano SI. J. Power Sources. 2014; 269:479.
12. Hwang JK, Lim HS, Sun Y, Suh KD. J. Power Sources. 2013; 244:538.
13. Poizot P, Laruelle S, Grugeon S, Dupont L, Tarascon JM. J. Power Sources. 2001; 97–98:235.
14. Laruelle S, Grugeon S, Poizot P, Dollé M, Dupont L, Tarascon JM. J. Electrochem. Soc. 2002; 149:A627.
15. Taberna PL, Mitra S, Poizot P, Simon P, Tarascon JM. Nat. Mater. 2006; 5:567. [PubMed: 16783360]
16. Lv PP, Zhao HL, Zeng ZP, Wang J, Zhang TH, Li XW. J. Power Sources. 2014; 259:92.
17. Wang ZY, Luan DY, Madhavi S, Li CM, Lou XW. Chem. Commun. 2011; 47:8061.
18. Hu P, Yu LJ, Zuo AH, Guo CY, Yuan FL. J. Phys. Chem. C. 2009; 113:900.
19. Wang B, Wu HB, Zhang L, Lou XW. Angew. Chem. Int. Ed. 2013; 52:4165.
20. Li L, Wang TT, Zhang LY, Su ZM, Wang CG, Wang RS. Chem. Eur. J. 2012; 18:11417. [PubMed: 22837077]
21. Zhang WM, Wu XL, Hu JS, Guo YG, Wan LJ. Adv. Funct. Mater. 2008; 18:3941.
22. Zhu T, Chen JS, Lou XW. J. Phys. Chem. C. 2011; 115:9814.
23. Chen JS, Zhang YM, Lou XW. ACS Appl. Mater. Interfaces. 2011; 3:3276. [PubMed: 21905690]
24. Yao TJ, Cui TY, Wang H, Xu LX, Cui F, Wu J. Nanoscale. 2014; 6:7666. [PubMed: 24899540]
25. Choi SJ, Kim MP, Lee SJ, Kim BJ, Kim ID. Nanoscale. 2014; 6:11898. [PubMed: 25175492]
26. Zhang XL, Fan ZH, Lu Q, Huang YL, Kaplan DL, Zhu HS. Acta Biomater. 2013; 9:6974. [PubMed: 23518477]
27. Fei X, Shao ZZ, Chen X. Nanoscale. 2013; 5:7991. [PubMed: 23863944]
28. Fei X, Jia MH, Du X, Yang YH, Zhang R, Shao ZZ, Zhao X, Chen X. Biomacromolecules. 2013; 14:4483. [PubMed: 24171643]
29. Fei X, Shao ZZ, Chen X. J. Mater. Chem. B. 2013; 1:213.
30. Yin GF, Huang ZB, Deng M, Zeng JW, Gu JW. J. Colloid Interf. Sci. 2011; 363:393.
31. Bai SM, Zhang XL, Lu Q, Sheng WQ, Liu LJ, Dong BJ, Kaplan DL, Zhu HS. Biomacromolecules. 2014; 15:3044. [PubMed: 25056606]
32. Lu Q, Wang XL, Lu SZ, Li MZ, Kaplan DL, Zhu HS. Biomaterials. 2011; 32:1059. [PubMed: 20970185]
33. Lin XH, Ji GB, Liu YS, Huang QH, Yang ZH, Du YW. Cryst Eng Comm. 2012; 14:8658.
34. Song Q, Zhang ZJ. J. Am. Chem. Soc. 2004; 126:6164. [PubMed: 15137781]

35. Sheng WQ, Liu J, Liu SS, Lu Q, Kaplan DL, Zhu HS. J. Mater. Chem. B. 2014; 2:7394.
36. Wang T, Porter D, Shao ZZ. Adv. Funct. Mater. 2012; 22:435.

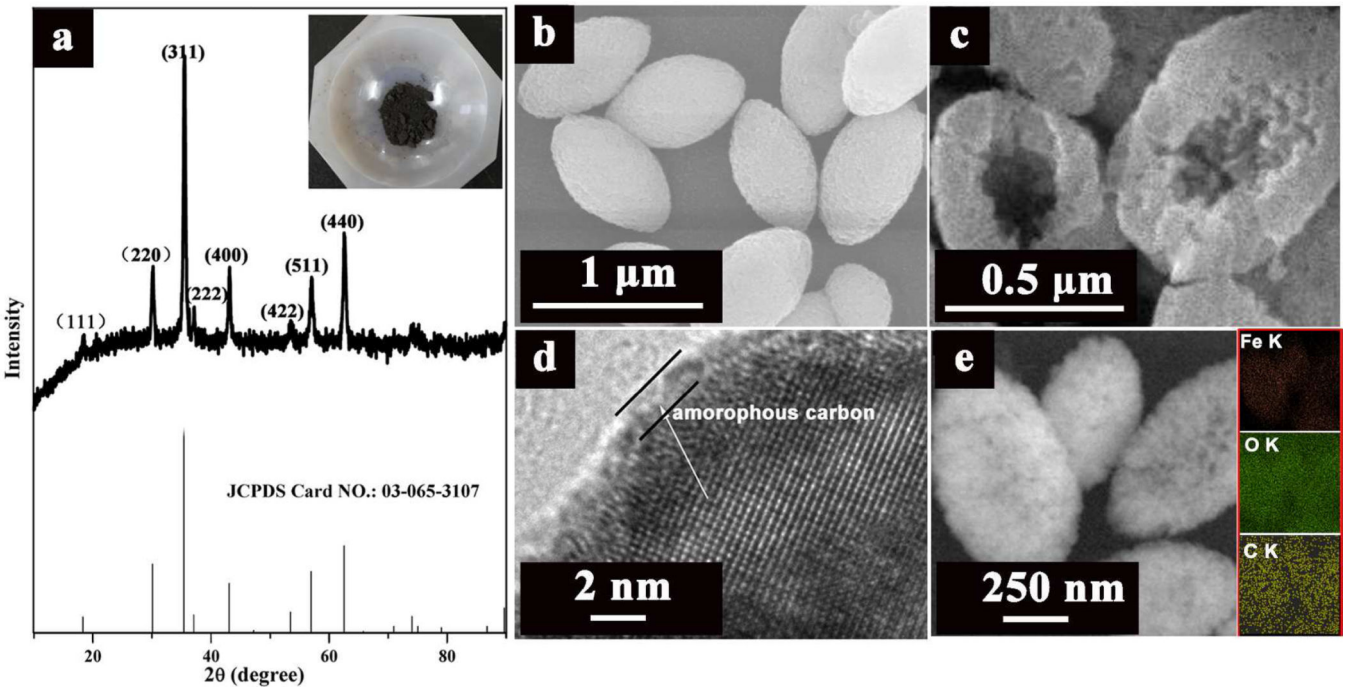

Figure 1.

XRD pattern (a), FESEM images (b, c, e) and HR-TEM image (d) of the obtained olive-like Fe_3O_4 hollow microspheres; insert in Figure 1a shows the optical image of the black coloured Fe_3O_4 in a mortar and the inserts in image of Figure 1e are the EDS mapping of Fe, O, and C according to the image of Figure 1e.

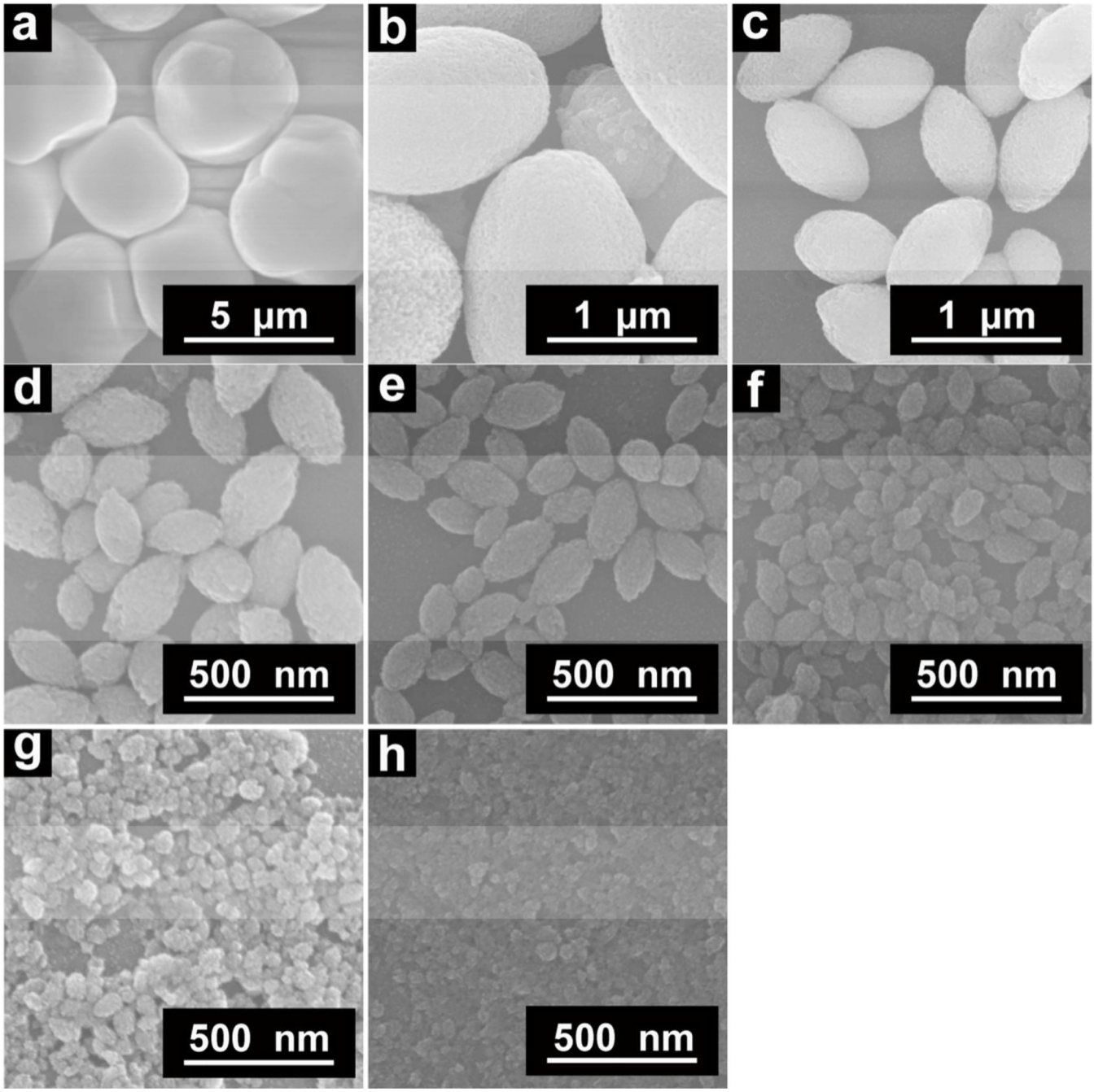

Figure 2.

FESEM images of the obtained olive-like α-Fe_2O_3 hollow microspheres prepared with different proportions (w/w) of SF to $FeCl_3 \cdot 6H_2O$. (a) 0, (b) 2:9, (c) 3:8, (d) 4:7, (e) 5:6, (f) 6:5, (g) 7:4, (h) 8:3.

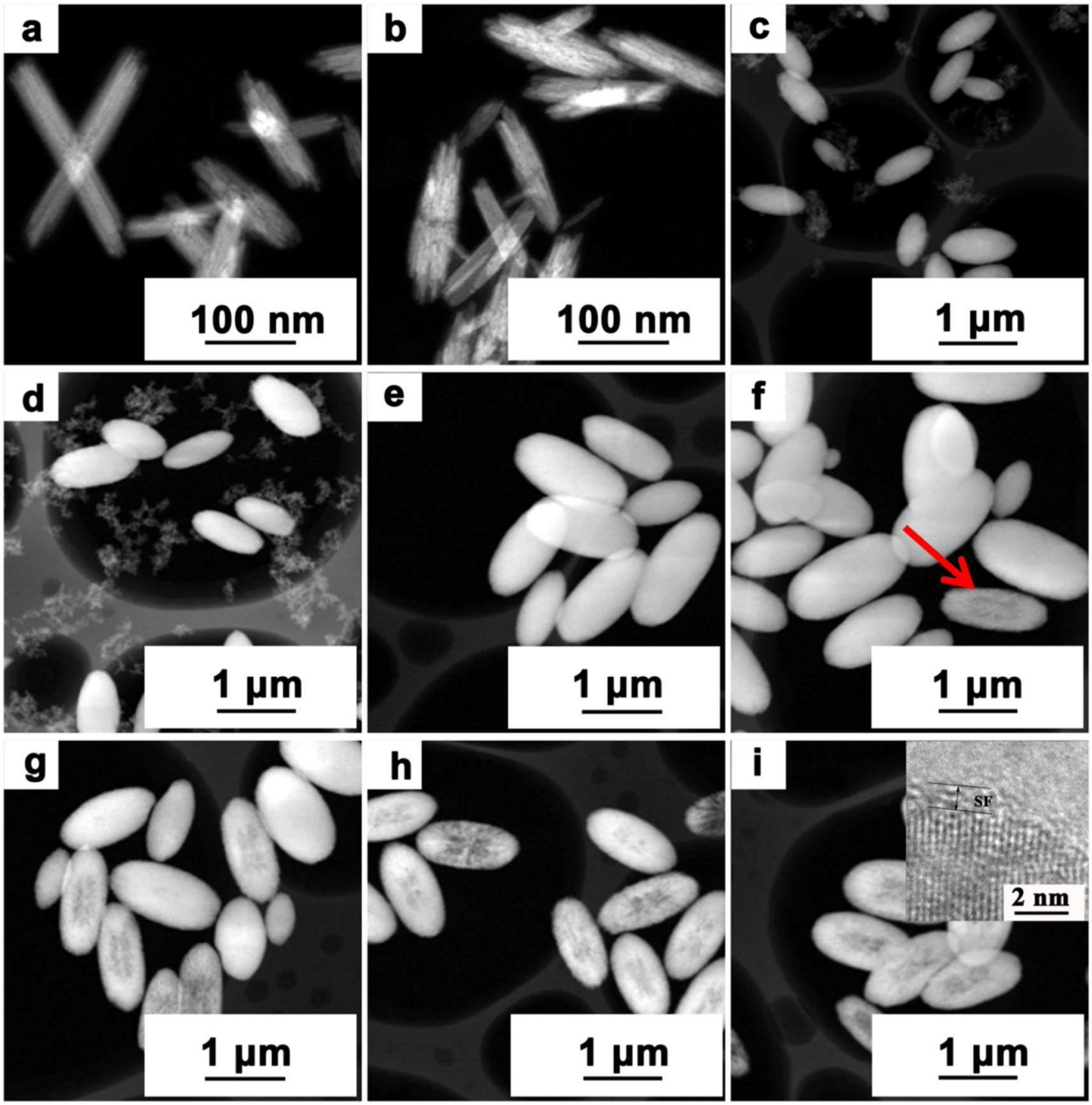

Figure 3.

HAADF-STEM images of the obtained olive-like α-Fe_2O_3/SF hollow microspheres prepared with different reaction time. (a) 1 h, (b) 2 h, (c) 3 h, (d) 4 h, (e) 6 h, (f) 8 h, (g) 12 h, (h) 20 h, (i) 24 h. The red arrow in Figure 6f indicates that the hollow structure began to form and the insert in Figure 6i is the HR-TEM image of the olive-like α-Fe_2O_3/SF hollow microspheres prepared with 24h, showing SF coating outside the olive-like α-Fe_2O_3/SF hollow microspheres.

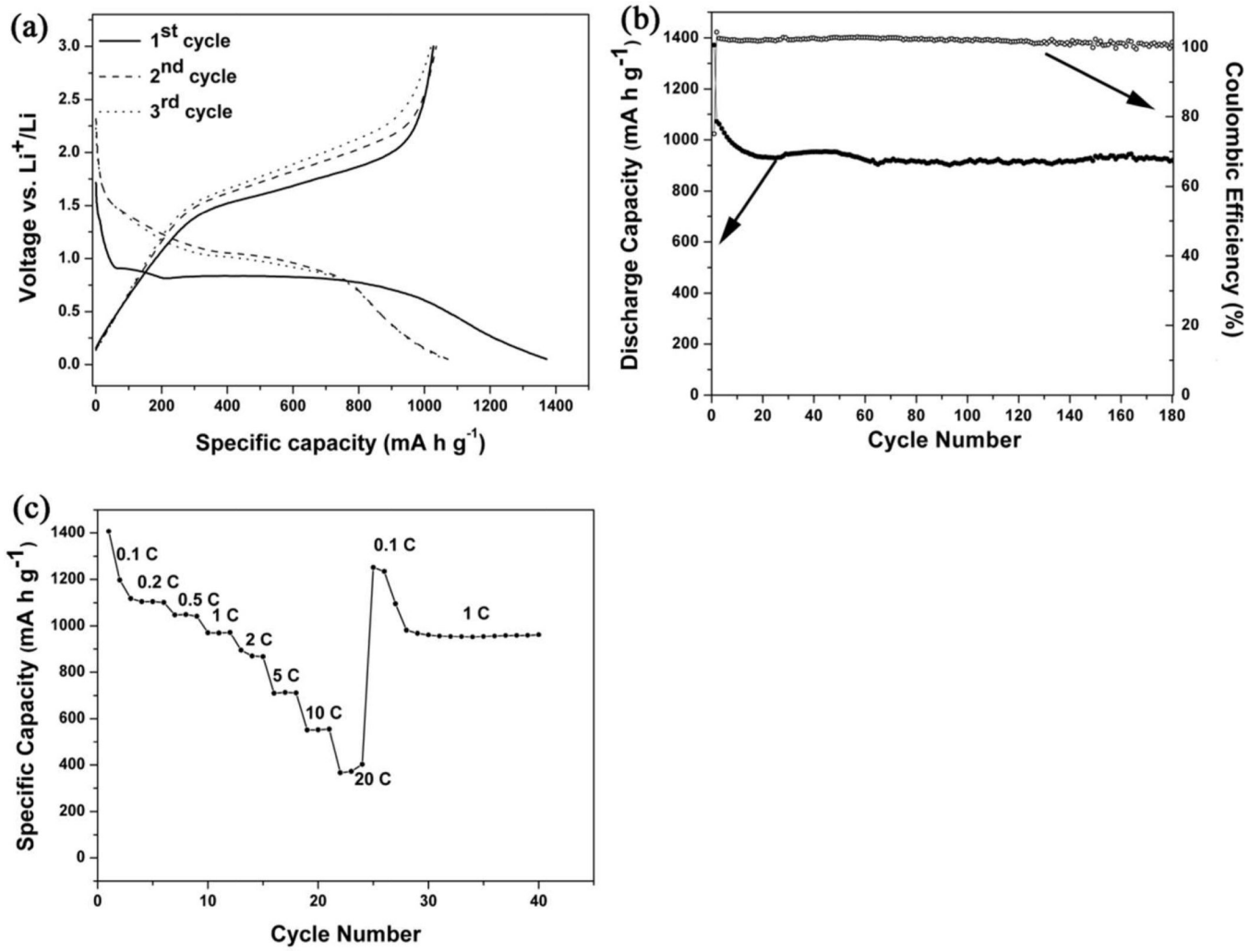

Figure 4.

(a) Charge-discharge curves and (b) cycling performance of olive-like hollow Fe_3O_4 electrode. All galvanostatic tests were performed at a constant current density of 0.2 C between 0.05 and 3 V (vs. Li^+5 /Li). (c) Rate performance of olive-like hollow Fe_3O_4 electrode at different rates ranging from 0.1 C to 20 C. (1 C=1000 mA g^{-1}).

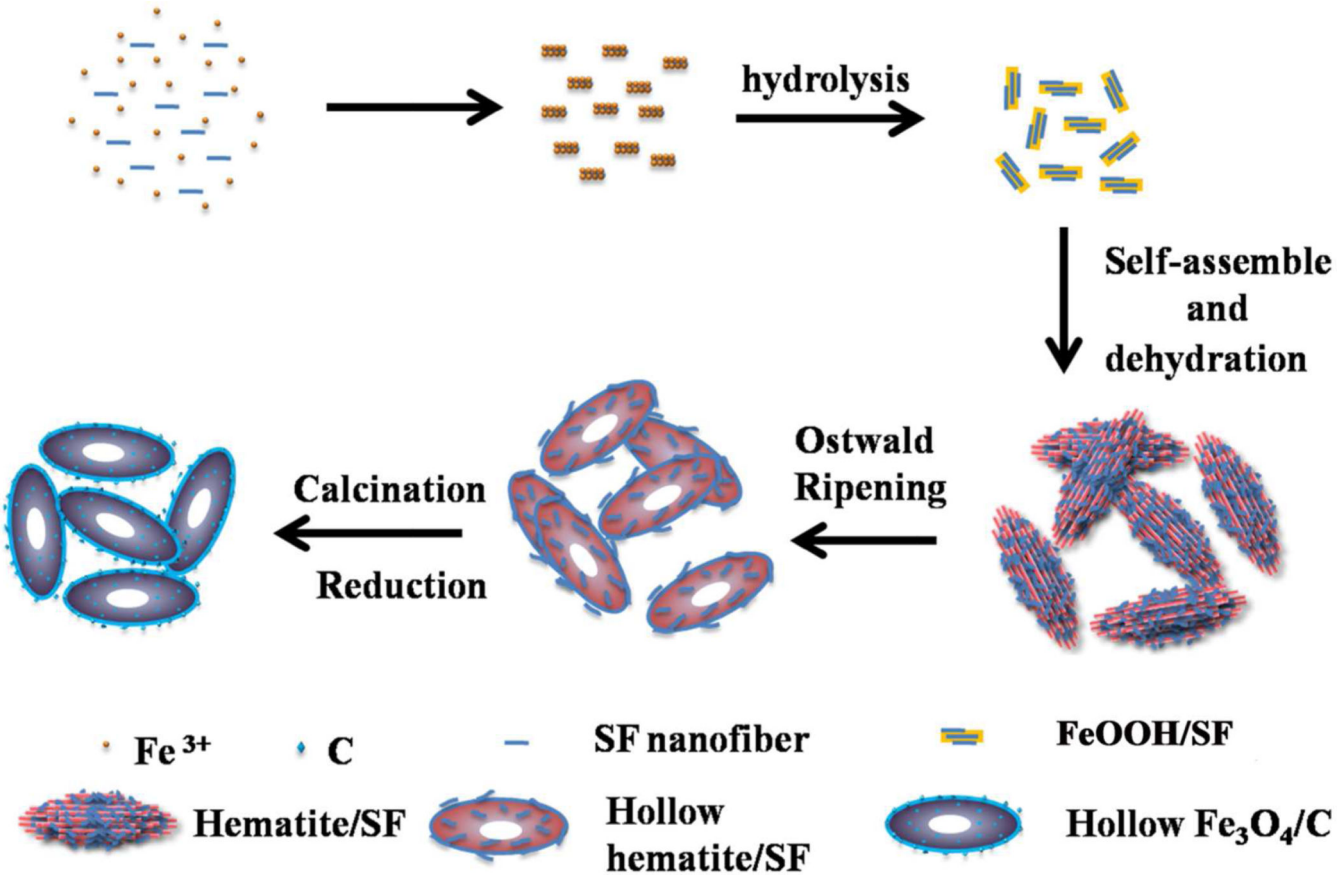

Scheme 1.

Possible mechanism for the formation of olive-like Fe_3O_4/C hollow microspheres.